ANNUAL REVIEWS

Annual Review of Marine Science

The History of Ocean Oxygenation

Christopher T. Reinhard[1,2,3] and Noah J. Planavsky[2,4]

[1]School of Earth and Atmospheric Sciences, Georgia Institute of Technology, Atlanta, Georgia 30332, USA; email: chris.reinhard@eas.gatech.edu

[2]Alternative Earths Team, Interdisciplinary Consortia for Astrobiology Research, National Aeronautics and Space Administration, Riverside, California 92521, USA

[3]Nexus for Exoplanet System Science (NExSS), National Aeronautics and Space Administration, Washington, DC 20546, USA

[4]Department of Earth and Planetary Sciences, Yale University, New Haven, Connecticut 06511, USA

Annu. Rev. Mar. Sci. 2022. 14:331–53

First published as a Review in Advance on August 20, 2021

The *Annual Review of Marine Science* is online at marine.annualreviews.org

https://doi.org/10.1146/annurev-marine-031721-104005

Keywords

biogeochemical cycles, ocean deoxygenation, nutrient cycling, atmospheric oxygen

Abstract

The large-scale dynamics of ocean oxygenation have changed dramatically throughout Earth's history, in step with major changes in the abundance of O_2 in the atmosphere and changes to marine nutrient availability. A comprehensive mechanistic understanding of this history requires insights from oceanography, marine geology, geochemistry, geomicrobiology, evolutionary ecology, and Earth system modeling. Here, we attempt to synthesize the major features of evolving ocean oxygenation on Earth through more than 3 billion years of planetary history. We review the fundamental first-order controls on ocean oxygen distribution and summarize the current understanding of the history of ocean oxygenation on Earth from empirical and theoretical perspectives—integrating geochemical reconstructions of oceanic and atmospheric chemistry, genomic constraints on evolving microbial metabolism, and mechanistic biogeochemical models. These changes are used to illustrate primary regimes of large-scale ocean oxygenation and to highlight feedbacks that can act to stabilize and destabilize the ocean–atmosphere system in anoxic, low-oxygen, and high-oxygen states.

1. INTRODUCTION

The atmosphere of the modern Earth contains ~20% molecular oxygen (O_2) by volume, making O_2 by far the most abundant constituent of Earth's atmosphere other than dinitrogen (N_2). This remarkably high O_2 abundance in the atmosphere represents a signal of Earth's surface biosphere that would be detectable from light years away (Meadows et al. 2018). Earth's oxygen-rich atmosphere also strongly impacts ocean chemistry, with the biogeochemistry of marine water columns and seafloor sedimentary environments being fundamentally regulated by the spatiotemporal distribution of dissolved O_2. The amount of metabolic energy available to a biosphere powered by O_2 is vast, such that the O_2-rich ocean–atmosphere system of the modern Earth supports staggering levels of standing biomass (Bar-On et al. 2018), energy flow (Falkowski et al. 2008), and ecological complexity (Steele 1974).

However, the abundance of O_2 in Earth's ocean–atmosphere system has changed dramatically as the Earth system has evolved (Canfield 2005, Kump 2008, Lyons et al. 2014). These changes span many orders of magnitude in atmospheric O_2 abundance and encompass a wide range of spatiotemporal scales. Some have been driven by major changes in the metabolic capacity of Earth's biosphere, while others have been pushed by external drivers of Earth's surface redox balance, such as the rate and style of volcanism and the modes of sediment burial in the oceans. Still others have been regulated by internal feedbacks within Earth's oceans that link together the abundance of O_2 in the ocean–atmosphere system, the fertility of the ocean biosphere, global climate, and the long-term exchanges of oxidized and reduced species between the solid and fluid Earth. Indeed, even today many regions of Earth's oceans are poised on the brink of anoxic conditions (Keeling et al. 2010), and such regions are often critically important for the large-scale biogeochemical cycles of many linked major and trace element species.

In what follows, we consider ocean oxygenation on Earth in the context of four major periods of Earth's history: (*a*) the Archean eon [4.0–2.5 billion years ago (Gya)], which bore witness to the earliest evolution of oxygen-producing organisms within the context of a pervasively reducing ocean–atmosphere system; (*b*) the early and middle Proterozoic eon (2.5–0.8 Gya), which saw the earliest stages of atmospheric and oceanic oxygenation; (*c*) the Neoproterozoic and Paleozoic eras [~800–250 million years ago (Mya)], which mark the dawn of the first complex aerobic ecosystems and perhaps the first pervasive oxygenation of Earth's oceans; and (*d*) the Mesozoic and Cenozoic eras (~250 Mya to the present day), a world marked by a stable, well-oxygenated ocean–atmosphere system that has nevertheless experienced large transient perturbations in ocean oxygenation. We begin by outlining the basic controls on ocean oxygenation, then discuss the current understanding of large-scale ocean oxygenation through each of these major periods of Earth's history. We consider each period from both theoretical and empirical perspectives and with an eye toward highlighting recent developments, current gaps in understanding, and interesting avenues for future work.

2. BASIC CONTROLS ON OCEAN OXYGENATION

In the modern oceans, the distribution of dissolved O_2 is principally regulated by the interaction between the supply of O_2 from the oxygen-rich atmosphere and the consumption of O_2 via aerobic respiration or the reduced species generated by anaerobic microbial metabolism. Dissolved O_2 concentrations in the modern surface ocean are thus uniformly high (**Figure 1*a***) and are largely within approximately ±5% of those predicted by equilibrium with the overlying atmosphere at in situ temperature and salinity (**Figure 1*c***). By contrast, large regions of the ocean interior can be strongly deficient in dissolved oxygen (**Figure 1*b*,*d***). Although a relative decrease in dissolved

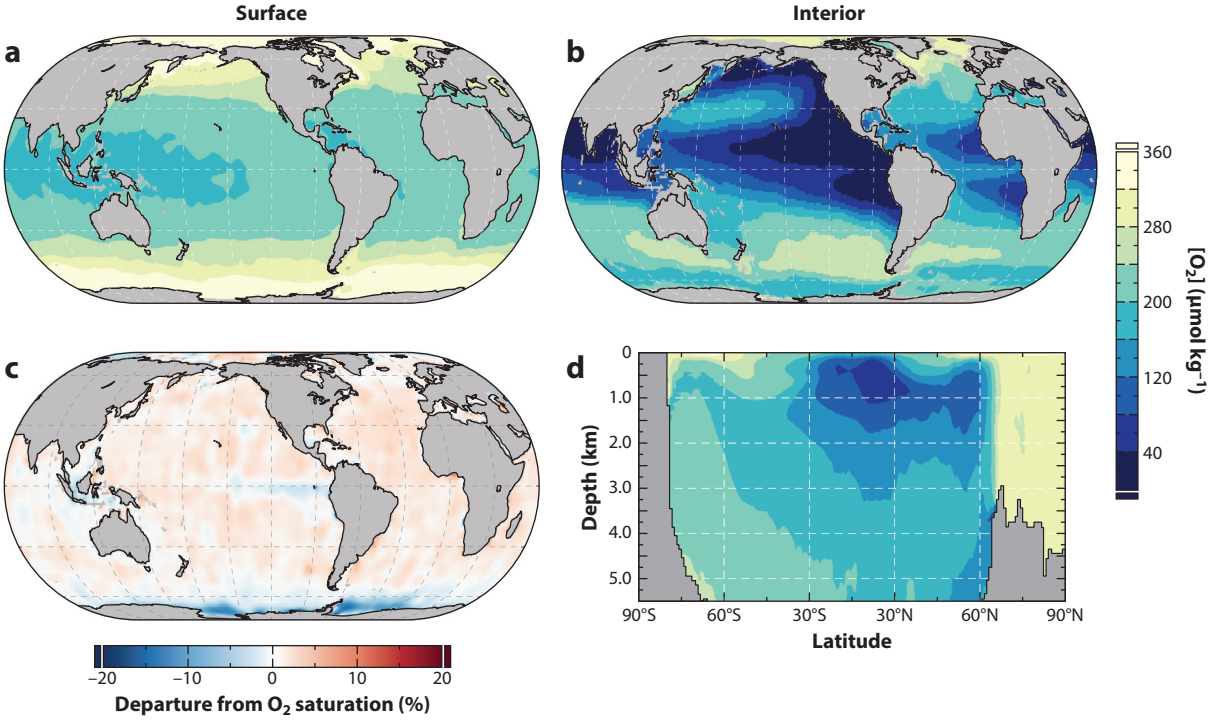

Figure 1

Dissolved [O_2] in the modern surface ocean and ocean interior. (*a*) Surface-ocean dissolved [O_2]. (*b*) Dissolved [O_2] at a depth of 525 m. (*c*) Percentage deviation from oxygen saturation in the surface ocean. (*d*) Zonally averaged latitudinal depth section of dissolved [O_2]. Note that the blue–green scale applies to panels *a*, *b*, and *d*, and the blue–red scale applies to panel *c*. Annually averaged data derived from the World Ocean Atlas 2018 (Boyer et al. 2018).

O_2 at intermediate depths is a pervasive feature in the ocean interior (Wyrtki 1962), particularly intense dissolved O_2 minima—or oxygen-deficient zones—are prominent features of the eastern tropical Pacific and Indian Oceans (**Figure 1*b***). In general, this pattern reflects intense respiratory consumption of O_2 combined with a relatively weak circulatory connection with the atmospheric O_2 reservoir via large-scale ocean circulation. Although the most intense oxygen-deficient zones represent a relatively small fraction of the overall modern ocean volume (e.g., Karstensen et al. 2008), they are in many cases functionally anoxic and are thus regions of significant importance for ocean metabolism and marine biogeochemistry (Wright et al. 2012). In the deeper oceans, limited respiratory demand and deep-water renewal result in relatively high deep-ocean dissolved O_2, particularly in regions of intense deep convection (e.g., the North Atlantic; **Figure 1*b*,*d***).

Throughout Earth's history, as is the case today, the oxygenation landscape of the oceans has been controlled by the balance between the supply of O_2 to the ocean interior and the distribution of respiratory demands within the ocean water column. These interactions can be visualized using a simple model that relates oxygen levels in the deep ocean to atmospheric O_2 abundance and the strength of the biological carbon pump—the production and transfer of organic carbon to the ocean interior by the marine biosphere. In this model (**Figure 2*a***), rates of O_2 supply to the deep ocean are controlled by the abundance of O_2 in the atmosphere and rates of ocean mixing, while rates of O_2 consumption in the ocean interior are controlled by bioavailable phosphorus (as PO_4^{3-}), which is assumed to govern steady-state organic carbon export flux from the surface

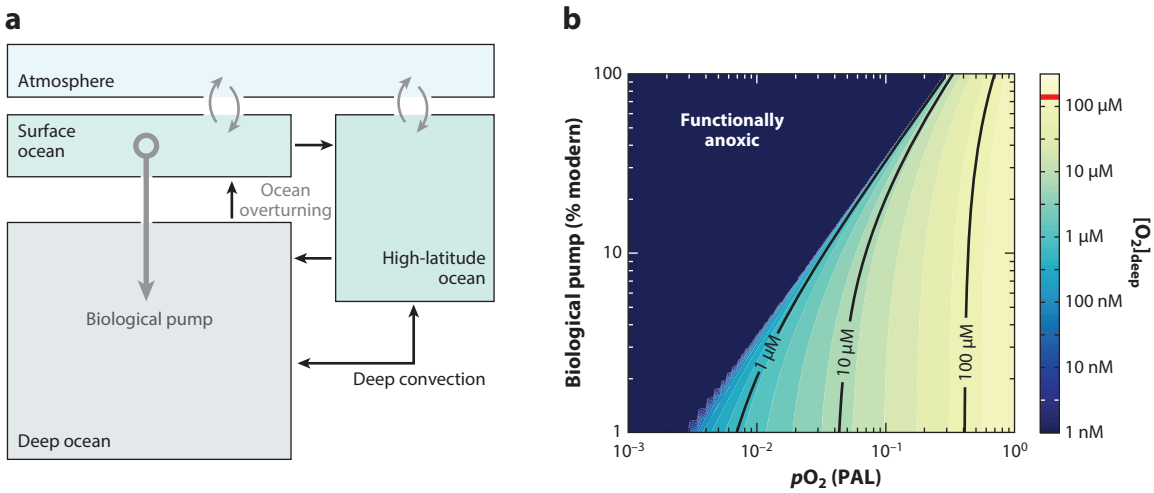

Figure 2

Conceptual model for deep-ocean oxygenation. (*a*) The model structure, showing key reservoirs and exchange fluxes between them. Boxes represent O_2 reservoirs, curved gray arrows represent air–sea gas exchange fluxes, and solid black arrows denote the meridional overturning circulation and deep convective mixing at high latitudes. Organic carbon is exported from the surface ocean by the biological pump at a magnitude commensurate with nutrient abundance in the ocean interior, creating an O_2 demand in the deep-ocean reservoir. (*b*) Oxygenation of the ocean interior as a function of atmospheric pO_2 and the strength of the ocean biological pump. Contours show steady-state dissolved O_2 concentration of the deep ocean ($[O_2]_{deep}$), and the red line shows the approximate value for the modern oceans. The term functionally anoxic refers here to $[O_2]_{deep}$ values below 1 nM. Abbreviations: PAL, present atmospheric level; pO_2, partial pressure of O_2.

ocean (Tyrrell 1999). The oxygenation of the model deep ocean is thus governed by the balance between O_2 supply from the atmosphere and O_2 demand by the marine biosphere, the latter of which is a function of ocean nutrient status.

Though clearly a simplification of the marine system, this model illustrates several important points. First, the partial pressure of O_2 (pO_2) in the atmosphere must be relatively high in order to maintain a pervasively ventilated deep ocean in the face of a biological pump similar to that of the modern Earth. For example, in this model, on the order of 30% of the present atmospheric O_2 level is required to maintain a deep-ocean $[O_2]$ above ~10 μmol kg^{-1} (**Figure 2*b***), while an average deep-ocean $[O_2]$ comparable to that of the modern deep ocean (~170 μmol kg^{-1}) requires an atmospheric pO_2 of at least ~50% that of the modern Earth regardless of the strength of the biological pump. Another key principle this model illustrates is that a drop in the marine nutrient inventory can counteract the impacts of lower atmospheric pO_2 on deep-ocean oxygenation. For instance, at a modern biological pump strength, a pervasively suboxic deep ocean—with dissolved $[O_2]$ on the order of 1 μmol kg^{-1}—occurs when atmospheric pO_2 drops below ~30% that of the modern Earth, but this condition can be maintained at atmospheric pO_2 values more than an order of magnitude below this if the marine nutrient inventory is sufficiently decreased (**Figure 2*b***).

An important fact that can be obscured by this style of analysis is that the abundance of atmospheric O_2 and marine nutrient inventory are not independent variables, because the global biogeochemical cycles of major nutrients fueling the biological pump (nitrogen, phosphorus, and a range of trace elements) are mechanistically linked to the oxygenation state of the ocean–atmosphere system. As a result, not all combinations of ocean nutrient inventory and atmospheric O_2 level are permissible at steady state, because many will be incapable of balancing long-term redox balance within the ocean–atmosphere–crust system. One of the simplest links among the

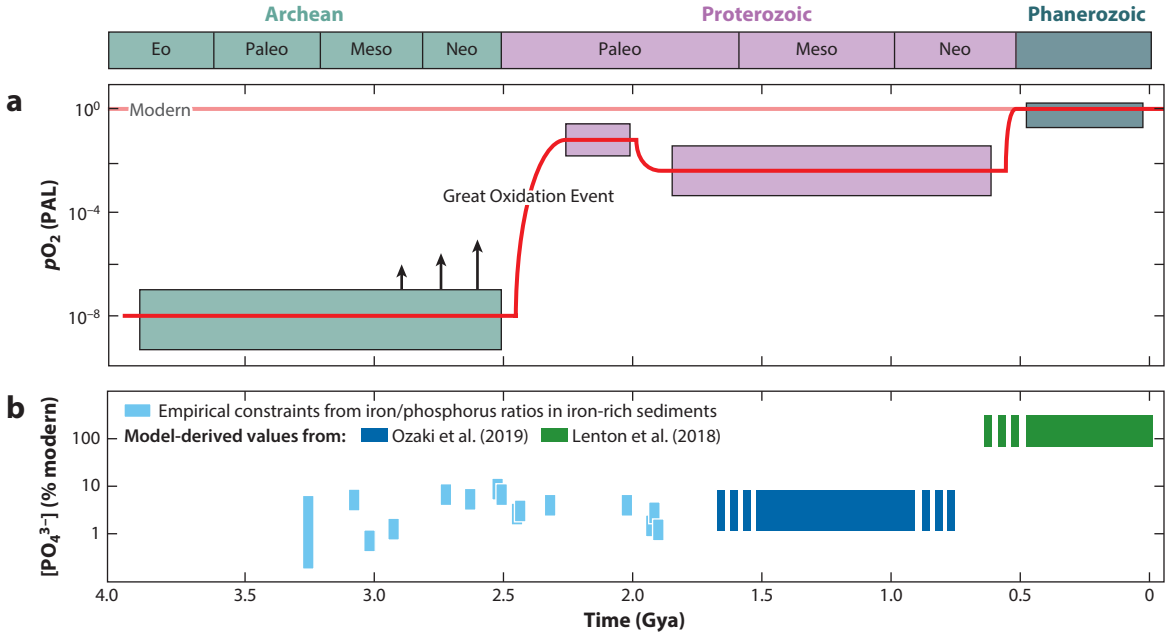

Figure 3

(*a*) Atmospheric pO_2 and (*b*) oceanic $[PO_4^{3-}]$ through Earth's history. In panel *a*, the boxes show approximate ranges consistent with existing geologic proxy constraints, and the solid line shows one plausible trajectory through them; the upward arrows depict putative transient increases in ocean–atmosphere O_2 abundance during the late Archean. In panel *b*, the small light blue bars show empirical constraints from iron/phosphorus ratios in iron-rich chemical sediments, and the larger bars (<1.8 Gya) show model-derived values from Ozaki et al. (2019) (*dark blue*) and Lenton et al. (2018) (*green*). Note that the absolute values and temporal trajectory of $[PO_4^{3-}]$ between approximately 1.8 and 0.5 Gya are not well constrained. Abbreviations: Gya, billion years ago; PAL, present atmospheric level; pO_2, partial pressure of O_2.

carbon, phosphorus, and O_2 cycles that has been explored in detail recently is that anoxic conditions favor increased organic carbon burial—which likely renders low-oxygen, high-productivity combinations unstable (Cole et al. 2021, Derry 2015, Laakso & Schrag 2017, Ozaki et al. 2019, Reinhard et al. 2017). Despite recent progress and its centrality to the operation of the Earth system, the quantitative scaling between atmospheric pO_2 and marine nutrient abundance (in particular PO_4^{3-}) is only broadly understood. In any case, it is useful to consider as a backdrop the long-term evolutionary trajectories of atmospheric pO_2 and ocean nutrient abundance (**Figure 3**), as these represent the key boundary conditions structuring ocean oxygenation through Earth's history (**Figure 2*b***).

3. OCEAN OXYGENATION AT THE DAWN OF OXYGENIC PHOTOSYNTHESIS: THE ARCHEAN EARTH

3.1. Oasis and Equilibrium Worlds

Prior to the evolution of oxygenic photosynthesis, the abundance of O_2 near Earth's surface would have been extremely low (Kasting et al. 1979). Photolytic and lightning-induced breakdown of CO_2, along with a disproportionation of H_2O_2 produced from photolysis of water vapor, would have yielded an average ground-level O_2 abundance on the order of 10^{-11} times the present atmospheric level (PAL) (Haqq-Misra et al. 2011). Following the evolution of oxygenic photosynthesis,

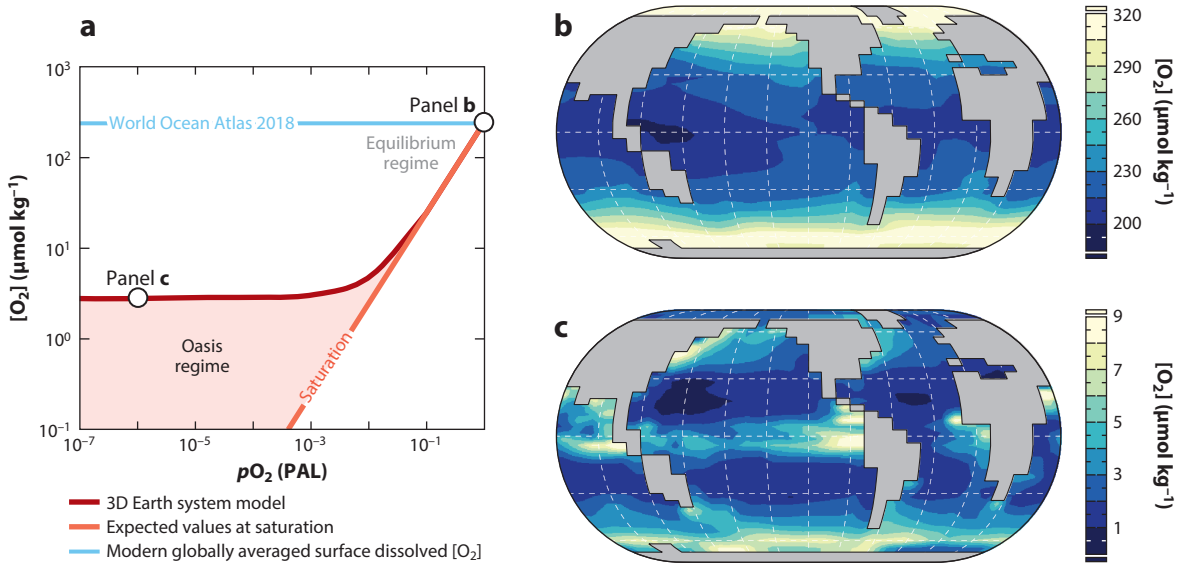

Figure 4

Dynamics of surface-ocean oxygenation as a function of atmospheric pO_2. Panel *a* illustrates globally averaged surface-ocean dissolved $[O_2]$ as a function of atmospheric pO_2, showing results from a three-dimensional Earth system model (*dark red line*) and expected values at saturation (*light red line*). The two are largely indistinguishable in the equilibrium regime, whereas in the oasis regime there is potential for significant local elevation in $[O_2]$ in the surface ocean (see also Olson et al. 2018). Shown for comparison is modern globally averaged surface dissolved $[O_2]$ from the World Ocean Atlas 2018 (Boyer et al. 2018) (*light blue line*). Circles show the individual states depicted in panels *b* and *c*; note the differing scales for $[O_2]$ in panels *b* and *c*. Abbreviations: PAL, present atmospheric level; pO_2, partial pressure of O_2.

atmospheric O_2 would have risen by many orders of magnitude (e.g., Kurzweil et al. 2013). However, the production and preservation of non-mass-dependent sulfur isotope anomalies (NMD-S) in Archean and earliest Paleoproterozoic sedimentary rocks indicate that atmospheric pO_2 was maintained at extremely low values, likely below $\sim 10^{-7}$ PAL, for most of Archean time (Farquhar et al. 2000, Pavlov & Kasting 2002, Zahnle et al. 2006) (**Figure 3*a***). At such low atmospheric pO_2 values, the ocean interior would have remained functionally anoxic, even at minuscule ocean nutrient abundances (**Figure 2*b***).

However, an extremely low-oxygen atmosphere does not necessarily imply a pervasively anoxic surface ocean (Kasting 1991, Olson et al. 2013, Reinhard et al. 2016). The emergence and ecological expansion of oxygenic photosynthesis would thus have given rise to two broad regimes of surface-ocean oxygenation (**Figure 4**). In the equilibrium regime—characteristic of the modern oceans—surface dissolved $[O_2]$ is governed largely by gas exchange equilibrium with the atmosphere. Globally averaged surface $[O_2]$ scales directly with atmospheric O_2 abundance (**Figure 4*a***) and broadly follows a latitudinal gradient in which $[O_2]$ is elevated in cold, high-latitude surface waters and decreases moving toward the equator (**Figure 4*b***). Local (and seasonal) gas exchange disequilibrium still exists (**Figure 1*c***), particularly in regions of deep convective mixing (Sun et al. 2017), but the disequilibrium is a small fraction of the overall oxygen reservoir and is superimposed on the latitudinal gradient driven largely by temperature-dependent solubility.

Below a certain threshold of atmospheric pO_2 the surface ocean enters the oasis regime, in which percentage shifts in surface dissolved $[O_2]$ can be highly variable, with some regions of the surface ocean effectively anoxic while others are characterized by local $[O_2]$ as high as ~ 10 μmol

kg^{-1} (**Figure 4*c***). Surface [O_2] tends to be locally elevated in coastal environments and regions of intense vertical nutrient exchange, which in a roughly modern ocean circulation regime include the major eastern boundary systems, the zone of equatorial divergence, and the Southern Ocean (**Figure 4*c***). The atmospheric pO_2 at which the surface ocean transitions between the oasis and equilibrium regimes will depend to some extent on the climate state and mean ocean circulation but should also respond to the ocean nutrient inventory. Specifically, as the ocean nutrient abundance drops, the oasis/equilibrium transition should shift to lower atmospheric pO_2.

The spatiotemporal dynamics and geomicrobiology of the surface ocean in the oasis regime are not fully understood, but the possibility of locally high dissolved [O_2] beneath a pervasively reducing atmosphere has several important implications. First, dissolved [O_2] on the order of 1 μmol kg^{-1} or more would be expected even if nutrient levels were relatively low, providing the potential for locally large redox-based energetic gradients for a wide range of microbial electron transfer and respiratory metabolisms. This is consistent with genomic evidence for a relatively rapid and comprehensive expansion of electron transfer pathways (David & Alm 2011) and oxygen-utilizing enzymes (Jabłońska & Tawfik 2021) during the Archean. Second, this regime of ocean oxygenation implies that oxygenic photosynthesis, along with an inclusive range of aerobic and high-potential electron transfer metabolisms, could exist in shallow-ocean environments while potentially remaining cryptic to geochemical tracers of atmospheric O_2 abundance. Tracking this ocean oxygenation regime may therefore also help to constrain the timing of perhaps the most significant biochemical innovation in the history of life on Earth—oxygenic photosynthesis.

3.2. Geologic Constraints on Surface-Ocean Oxygenation During the Archean Eon

As discussed above, the preservation of NMD-S signals in Archean sedimentary rocks indicates extremely low atmospheric O_2, and these signals are pervasive throughout the Archean and Paleoproterozoic rock record (e.g., Johnston 2011). Massive iron formations—many of which appear to have formed under a water column in which iron was always more abundant than oxygen (Busigny et al. 2014, Planavsky et al. 2012)—also indicate essentially oxygen-free oceans during some periods of Archean time. At the same time, however, there is evidence for the local accumulation of dissolved O_2 in surface-ocean environments prior to the initial oxygenation of Earth's atmosphere. Particularly striking are significant enrichments in solid-phase manganese, along with co-occurring enrichments in ^{95}Mo, in iron-rich sedimentary rocks from the Sinqeni Formation (Mozaan Group, South Africa) deposited at ~3.0 Gya (**Figure 5**). Petrographic, geochemical, sedimentological, and isotopic data all suggest rapid and effective production, stabilization, and delivery of manganese mineral phases to sediments during the deposition of the Sinqeni Formation (Ossa Ossa et al. 2016, 2018; Planavsky et al. 2014). This has been interpreted to reflect the oxidation of dissolved manganese and stabilization of manganese oxides in the presence of dissolved O_2, followed by delivery to sediments and diagenetic recycling to manganese-bearing carbonate phases. Similar geochemical signatures are also observed in slightly younger Archean iron formations (Kurzweil et al. 2016). This interpretation of sediment manganese enrichments is robust regardless of the possibility of oxygen-free manganese oxidation—through UV photooxidation (Anbar & Holland 1992), photosynthetic oxidation (Johnson et al. 2013), or oxidation with elemental sulfur (Daye et al. 2019)—given rapid manganese reduction under anoxic conditions (e.g., Busigny et al. 2014).

Additional evidence for the accumulation of O_2 in shallow-ocean environments can be found in younger siliciclastic and iron-rich marine sedimentary rocks deposited between approximately 2.7 and 2.5 Gya in western Australia and South Africa. In particular, bulk rock and kerogen-bound

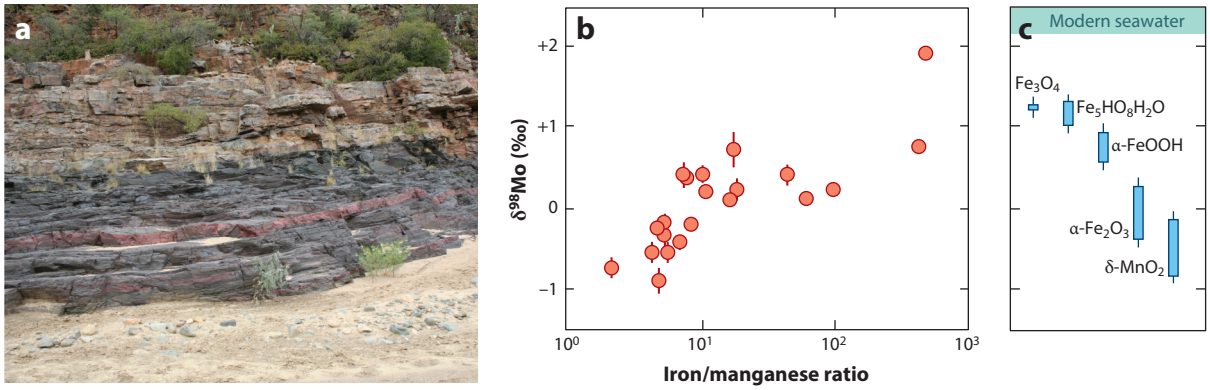

Figure 5

Geologic evidence for early oxygenic photosynthesis. (*a*) Banded iron formation and ferruginous shale of the Vlakhoek Member unconformably overlain by the Kwaaiman Member in the Mozaan Group, South Africa. (*b*) Stable molybdenum isotope compositions of iron-rich samples from the Mozaan Group [$\delta^{98}Mo = ({}^{98}R_{samp}/{}^{98}R_{std} - 1) \times 1{,}000$] as a function of iron/manganese ratio, showing the characteristic enrichment in $\delta^{98}Mo$ as manganese content increases. (*c*) Experimentally derived isotope effects associated with sorption of dissolved MoO_4^{2-} onto a range of iron- and manganese-oxide mineral phases. The most negative $\delta^{98}Mo$ compositions observed in Archean sediments are consistent with the delivery of manganese-oxide phases to the sediments and thus imply appreciable dissolved O_2 in surface-ocean environments. Photo in panel *a* adapted with permission from Ossa Ossa et al. (2016); data in panels *b* and *c* taken from Planavsky et al. (2014) and Goldberg et al. (2009), respectively.

stable nitrogen isotopes in organic-rich shales from the ~2.7-Gya Jeerinah Formation and the ~2.5-Gya Mt. McRae Shale (Hamersley Group, western Australia), along with the ~2.6-Gya Nauga Formation (Ghaap Group, South Africa), are consistent with the presence of coupled nitrification and denitrification (or anaerobic ammonium oxidation) reactions in some shallow marine environments (Garvin et al. 2009, Godfrey & Falkowski 2009, Koehler et al. 2018), strongly suggesting the presence of dissolved O_2. In the Nauga Formation, these observations co-occur with evidence from stable iron isotopes for partial iron oxidation (Czaja et al. 2012). Observations from stable thallium isotopes in the Mt. McRae Shale suggest burial of oxidized manganese in shallow-ocean sediments at ~2.5 Gya (Ostrander et al. 2019), consistent with a range of stable isotopic, trace element, and radiogenic isotope data suggesting transient but possibly significant accumulations of surface O_2 in the late Archean Earth system (Anbar et al. 2007, Kendall et al. 2015a). Importantly, all of these signals co-occur with significant NMD-S anomalies, suggesting the continued presence of a pervasively O_2-poor atmosphere (Kaufman et al. 2007, Ono et al. 2009).

It is difficult to definitively rule out alternative mechanisms for producing any individual geochemical signature, particularly in sedimentary rocks that have long and complex post-depositional histories at or near Earth's surface. In particular, alternative pathways for partial iron oxidation and significant nitrogen isotope fractionation that do not require the presence of O_2 should also be considered, including oxidation of iron by anoxygenic photosynthetic bacteria (e.g., Croal et al. 2004) and nitrogen isotope redistribution due to partial uptake of NH_4^+ and/or coupling with anoxic iron redox cycling (Busigny et al. 2013). These considerations highlight the importance of combining multiple independent lines of evidence and interpretation in the fullest possible environmental context. Nevertheless, the collective Archean geochemical record points to a surface-ocean oxygenation landscape in the oasis regime during at least some periods of the Archean, and possibly sporadically more intense ocean oxygenation leading up to a major shift in ocean–atmosphere redox state during the early Proterozoic.

4. FEAST AND FAMINE: RISING AND FALLING OXYGEN AND PRODUCTIVITY ON THE PROTEROZOIC EARTH

4.1. Ocean Oxygenation in the Wake of the Great Oxidation Event

A wide range of observations from Earth's rock record indicate a transition to a more oxidizing Earth surface environment after ~2.3 Gya—the Great Oxidation Event (Bekker et al. 2005 and references therein). How much atmospheric O_2 rose initially during this period is not entirely clear. Photochemical models indicate that pO_2 must be above $\sim 10^{-5}$ PAL to prevent the production and delivery of NMD-S anomalies near Earth's surface (Pavlov & Kasting 2002, Zahnle et al. 2006). This is generally consistent with an apparent loss of detrital reduced minerals from coarse-grained coastal fluvial and marine sediments (Johnson et al. 2014, Rasmussen & Buick 1999, Roscoe & Minter 1993) and evidence for iron oxidation in the terrestrial realm (Holland 1984, Rye & Holland 1998). However, all of these observations are consistent with an atmospheric pO_2 perhaps orders of magnitude below what should be required to ventilate large regions of the ocean interior (**Figure 2*b***). Stable nitrogen isotope data indicate the onset of a pervasive aerobic nitrogen cycle in the surface ocean during this interval (Luo et al. 2018, Zerkle et al. 2017), but it is not straightforward to tie this quantitatively to an atmospheric O_2 value or global ocean oxygenation landscape.

Accumulating sedimentological and geochemical observations suggest a transient period of elevated atmospheric O_2 between approximately 2.2 and 2.0 Gya (**Figure 3*a***) in association with a very large perturbation to Earth's carbon cycle (Karhu & Holland 1996). Anomalously positive carbon isotope records during this time period—whether they track a local or global signal (Geyman & Maloof 2019, Karhu & Holland 1996)—likely point to high rates of primary productivity. The oldest bedded sulfate evaporite deposits in Earth's rock record also appear during this interval, in the Lucknow Formation in South Africa (Schröder et al. 2008) and the Tulomozero Formation in northwest Russia (Melezhik et al. 2005). The formation of gypsum (a hydrated sulfate mineral, $CaSO_4{\cdot}2H_2O$) before halite (NaCl) in these systems implies seawater sulfate concentrations above ~1–2 mmol kg^{-1} (compared with 28 mmol kg^{-1} in modern seawater). The stable calcium isotope composition of Tulomozero evaporites, together with the presence of magnesium sulfate minerals, further constrains contemporaneous seawater to contain at least ~10 mmol kg^{-1} (Blättler et al. 2018). While this does not provide a direct constraint on ocean–atmosphere O_2 levels, it is indicative of a robust oxidative sulfur cycle and is consistent with pervasive oxygenation of Earth's oceans. For instance, ocean-sediment models of global sulfur cycling imply that these sulfate levels require largely oxygenated oceans (Fakhraee et al. 2019).

Redox-sensitive trace elements, sedimentary iron speciation, and stable molybdenum isotope systematics in the Francevillian Group in western Africa suggest local ocean oxygenation beneath storm wave base (e.g., on the order of 10–100 m) at ~2.1–2.0 Gya (Canfield et al. 2015). Marked redox-sensitive trace element and ^{238}U enrichments in siliciclastic sedimentary rocks from the slightly younger Zaonega Formation in northwest Russia provide additional evidence of widespread ocean oxygenation at ~2.0 Gya (Mänd et al. 2020). As above, quantitative links between redox-sensitive trace element enrichments and stable isotope systematics remain imprecise, making it difficult to use these data to definitively constrain atmospheric pO_2 and large-scale patterns of ocean oxygenation. However, taken together with quantitative estimates of elevated seawater SO_4^{2-}, these observations point toward pervasive ocean oxygenation, perhaps on a scale comparable to that of the recent/modern Earth.

There is evidence for a relatively rapid drop in ocean–atmosphere oxygen levels and marine primary production following this apparent period of transient ocean oxygenation. This shift in redox conditions is marked foremost by the reappearance of evidence for anoxic conditions in very

shallow waters and the disappearance of sulfate evaporites (Canfield 2005, Grotzinger & Kasting 1993). Most notably, between 1.9 and 1.8 Gya (Fralick et al. 2002) there was an apparent return to the deposition of massive shallow-water iron formations, with iron oxidation occurring in the wave-mixed upper portion of the oceans (Dimroth & Chauvel 1973, Planavsky et al. 2009, Raye et al. 2015). There is also evidence from rare-earth element systematics for anoxic conditions in very shallow water (likely >50 m) (Bellefroid et al. 2018). These observations are consistent with recent oxygen isotopic evidence for a dramatic drop in oceanic primary production after ~2 Gya (Hodgskiss et al. 2019).

4.2. An Oligotrophic Ocean Model for the Mid-Proterozoic Earth

Existing constraints on ocean oxygenation during the mid-Proterozoic (~1.8–0.8 Gya) yield complex and variable signals. The speciation of iron-bearing minerals in marginal siliciclastic sedimentary rocks (Guilbaud et al. 2015, Planavsky et al. 2011, Poulton et al. 2010, Sperling et al. 2015) suggests that anoxic bottom waters were common on shelf and slope environments but were buffered by dissolved Fe^{2+} rather than hydrogen sulfide (termed ferruginous conditions). The contrasting behaviors of molybdenum, chromium, uranium, and rhenium in organic-rich marginal sedimentary rocks deposited throughout the mid-Proterozoic qualitatively indicate widespread marine anoxia (Partin et al. 2013, Reinhard et al. 2013, Scott et al. 2008, Sheen et al. 2018) and, when coupled to mass balance modeling of oceanic trace element inventories, suggest that the most common form of anoxia in modern oceans—euxinia (anoxic but containing dissolved H_2S)—covered only a very small fraction of the seafloor (Reinhard et al. 2013). In addition, there are geochemical signals for anoxic conditions in very-shallow-water environments, including in the wave-mixed portions of the oceans (Bellefroid et al. 2019, Doyle et al. 2018, Liu et al. 2021, Tang et al. 2016). Taken together, these observations indicate pervasively anoxic, but sulfur-poor, ocean chemistry for much of mid-Proterozoic time.

However, several observations point to surface-ocean oxygenation and a heterogeneous marine redox landscape at intermediate depths in mid-Proterozoic oceans. For example, multiproxy investigation of the ~1.8-Gya Stambaugh Formation in the United States indicates episodic deep-water oxygenation against a background of predominantly anoxic conditions (Planavsky et al. 2018b). Limited reactive iron enrichment and muted enrichment of redox-sensitive trace elements in basinal shales from the Kaltasy Formation in central Russia (~1.4 Gya) are consistent with at least weakly oxygenated conditions in some deep-shelf environments contemporaneous with euxinic and ferruginous conditions in similar depositional environments elsewhere (Sperling et al. 2014). Authigenic iodine enrichments in shallow marine carbonates and early diagenetic carbonate concretions also suggest widespread oxygenation of the upper oceans during some intervals of the mid-Proterozoic (Liu et al. 2020, Shang et al. 2019).

True archives of deep-ocean oxygenation prior to the Cenozoic (65 Mya to the present) are extremely rare. Volcanogenic massive sulfide deposits, often containing iron-rich chemical sediments and associated sulfide ores rich in copper, provide one of the few windows into true deep-ocean chemistry during mid-Proterozoic time (Slack et al. 2007). Importantly, the copper-rich composition of these deposits requires hydrostatic pressure equivalent to a depth of at least ~1 km to prevent loss of copper prior to mineralization at the seafloor (Slack et al. 2007, 2009). The trace and rare-earth element systematics of similar volcanogenic massive sulfide deposits formed at approximately 1.8 Gya, 1.7 Gya, 1.4 Gya, and 1.2 Gya have been interpreted to reflect weakly oxygenated (suboxic) conditions in the deep ocean for at least some periods of the mid-Proterozoic (Little et al. 2021; Slack et al. 2007, 2009). Evidence for low-oxygen conditions is consistent with

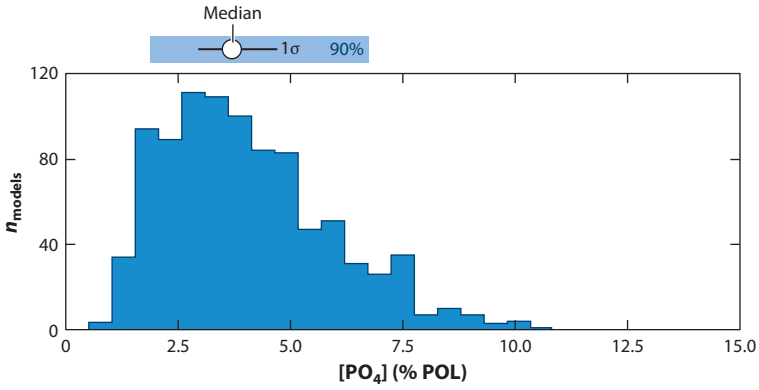

Figure 6

Statistical distribution of deep-ocean dissolved [PO_4^{3-}] during the mid-Proterozoic derived from the stochastic large-ensemble model analysis of Ozaki et al. (2019). The histogram shows the distribution of individual model runs, the open circle denotes the median value, the solid line shows ±1σ, and the shaded bar shows the 90% credible interval. Abbreviation: POL, present oceanic level (~2.1 μmol kg^{-1}).

deep-ocean [O_2] reconstructed from the iron redox chemistry of extrusive, subaqueous volcanic rocks, though this record also allows for pervasive deep-ocean anoxia (Stolper & Keller 2018), and the eruption depths of these rocks are not always well constrained.

As discussed above, estimates of both biospheric productivity and atmospheric O_2 are needed in order to fully understand the factors controlling ocean oxygenation. Although the precise range of atmospheric pO_2 values during the mid-Proterozoic is not yet clear (Gregory et al. 2021, Liu et al. 2021, Planavsky et al. 2018a), it is widely accepted that atmospheric O_2 was well below that of the modern Earth. At the same time, there is increasing evidence from both the rock record and biogeochemical models indicating very low marine nutrient abundances—and thus levels of primary productivity—during the same period. In particular, the abundance of phosphorus in siliciclastic sedimentary rocks deposited along continental margins throughout the mid-Proterozoic has been interpreted to reflect extreme phosphorus-limited growth and very little phosphorus authigenesis even in biogeochemically active, organic-rich continental margin sediments (Reinhard et al. 2017). In parallel, large-ensemble biogeochemical modeling (Ozaki et al. 2019) suggests a mid-Proterozoic PO_4^{3-} inventory on the order of 5% of the present oceanic level (**Figure 6**), consistent with results from low-order Earth system models (e.g., Laakso & Schrag 2017). A low-productivity marine biosphere is also consistent with the stable oxygen isotope compositions of marine and lacustrine evaporite minerals, which have been interpreted to suggest reduced biospheric productivity during the mid-Proterozoic (Crockford et al. 2018).

Altogether, Earth's mid-Proterozoic rock record provides evidence for an oligotrophic ocean in which the ocean redox structure is maintained in a mixed anoxic/weakly oxygenated state at relatively low atmospheric pO_2 and low marine nutrient abundance. The first-order features of ocean oxygenation under these conditions can be broadly illustrated by implementing the estimated marine PO_4^{3-} abundances obtained by Ozaki et al. (2019) in a three-dimensional ocean biogeochemistry and climate model, assuming a roughly modern ocean bathymetry and climate state but a much lower atmospheric pO_2 of 1% PAL (**Figure 7**). We consider three scenarios for each of the bounded PO_4^{3-} inventory values obtained by Ozaki et al. (2019): (*a*) a default scenario, with a mean climate and ocean circulation similar to that of the modern Earth; (*b*) a high-CO_2 scenario, in which atmospheric pCO_2 is set to 10 times that of the modern preindustrial value; and

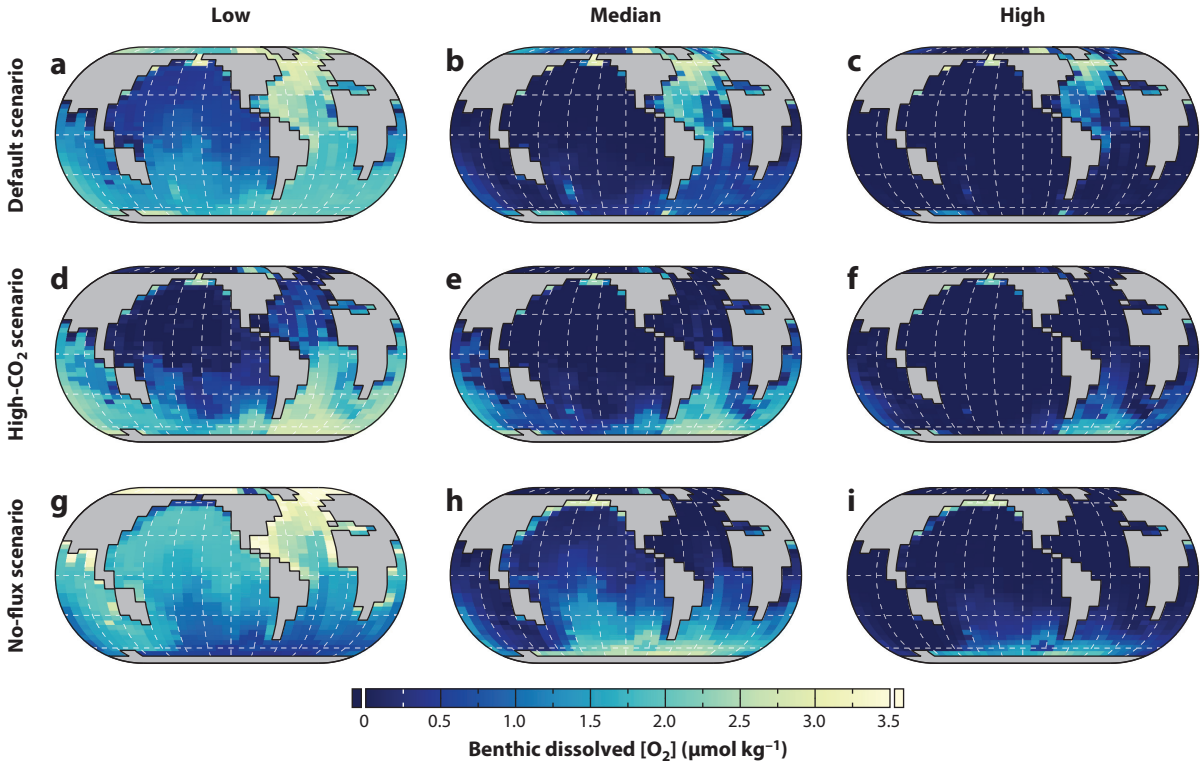

Figure 7

Benthic dissolved [O_2] in a three-dimensional Earth system model forced with estimated mid-Proterozoic nutrient abundances and an imposed low atmospheric pO_2 of 1% PAL. (*a–c*) The default case, with a preindustrial atmospheric pCO_2 and climate state. (*d–f*) A high-CO_2 case, in which atmospheric pCO_2 is arbitrarily increased to 10 times the PAL and the climate state is allowed to respond accordingly. (*g–i*) A no-flux case, in which the intensity of the meridional overturning is arbitrarily reduced by eliminating a default prescribed freshwater rebalancing flux (see Marsh et al. 2011). Columns depict results for the lower 90% credible interval (low), the median value (median), and the upper 90% credible interval (high) shown in **Figure 6**. Abbreviations: PAL, present atmospheric level; pO_2, partial pressure of O_2.

(*c*) a no-flux scenario, in which the freshwater rebalancing flux in the ocean circulation model is adjusted downward, decreasing the strength of the meridional overturning circulation (e.g., Marsh et al. 2011).

The spatial patterns of benthic ocean oxygenation resulting from this exercise are shown in **Figure 7**. We emphasize that this analysis is only meant to be illustrative—bathymetry, climate state, and ocean nutrient abundance are only weakly constrained for this period of Earth's history and would also have changed considerably over time. Nevertheless, it demonstrates that, in principle, large regions of the seafloor can be weakly oxygenated even at a relatively low atmospheric pO_2 of ~1% PAL, with large regions of the deep ocean characterized by dissolved [O_2] on the order of micromoles per kilogram of seawater. This redox state would be difficult to distinguish from oxic depositional conditions using iron speciation or trace element enrichments (Scholz 2018, Sperling et al. 2014) and is fully consistent with constraints based on stable uranium isotope systematics (Yang et al. 2017) and the geochemistry of deep-sea volcanogenic massive sulfide deposits (Slack et al. 2007, 2009). Such a weakly oxygenated state can also be maintained at progressively higher marine nutrient abundances provided that atmospheric pO_2 also rises (**Figure 2*b***).

Placing more definitive constraints on atmospheric pO_2 and marine nutrient abundance during the mid-Proterozoic remains an important challenge. It is particularly important to better establish the quantitative scaling between ocean–atmosphere O_2 levels and marine nutrient abundance, which is currently only crudely parameterized in biogeochemical models (Laakso & Schrag 2017, Ozaki et al. 2019, Reinhard et al. 2017). The development of ocean biogeochemistry models with more robust mechanistic representations of the coupled oceanic cycles of iron, phosphorus, and sulfur represents a significant challenge (van de Velde et al. 2021) but will be critical in future attempts to invert patterns of ocean oxygenation for atmospheric composition. Despite key advances in using iron-rich chemical sediments to develop first-order constraints on marine [PO_4^{3-}] through time (Bjerrum & Canfield 2002, Jones et al. 2015, Konhauser et al. 2007), there is also a pressing need to develop additional empirical constraints on both marine nutrient levels and marine primary production. Nevertheless, we suggest that the working hypothesis of an oligotrophic ocean state may help to reconcile geologic evidence for low atmospheric pO_2 with the current understanding of spatial redox structure and evidence for weakly oxygenated conditions from existing archives of deep-ocean chemistry.

5. VENTILATING THE OCEAN INTERIOR: THE NEOPROTEROZOIC AND EARLY PHANEROZOIC EARTH

It is common to depict the oxygenation of Earth's ocean–atmosphere system as having occurred in two broadly stepwise increases near the beginning and end of the Proterozoic eon (Canfield 2005, Lyons et al. 2014, Och & Shields-Zhou 2012) (**Figure 3**). However, in detail, both of these transitions were likely dynamic and complex in their own right. In particular, although there are multiple instances of apparent late Neoproterozoic ocean oxygenation on a broad scale (Kendall et al. 2015b; Sahoo et al. 2012, 2016), it is becoming increasingly clear that there was not a single transition to a more oxygenated ocean state. Geochemical and sedimentological records instead suggest multiple instances of widespread ocean oxygenation against a backdrop of largely anoxic oceans during most of the late Neoproterozoic era.

There is also increasing evidence that ocean anoxia was extensive in the early Paleozoic era, an idea with a long history (Berry & Wilde 1978, Wilde 1987). Specifically, combined evidence from local (Sperling et al. 2015), regional (Lu et al. 2018, Wallace et al. 2017), and global (Dahl et al. 2019, Wei et al. 2020) redox proxies suggests extensive anoxia during the Cambrian (~541–485 Mya), Ordovician (~485–444 Mya), and Silurian (~444–420 Mya). Similar to the Neoproterozoic, there are intervals—particularly during the Cambrian—during which the extent of marine anoxia appears to have waxed and waned periodically. For instance, sulfur and uranium isotope systematics indicate multiple intense spikes in the pervasiveness of marine anoxia during the early (~530 Mya) and late (~500 Mya) Cambrian (Dahl et al. 2019, Gill et al. 2011), while there appear to have been transient intervals of ocean oxygenation intensity that may have been similar to that of the modern Earth (Dahl et al. 2019). The general picture is one of progressive, if fitful, ocean oxygenation through the late Neoproterozoic and Paleozoic eras, with ocean oxygenation landscapes starting to become broadly similar to that of the modern/recent Earth only after ~400 Mya.

The apparent expansion of well-oxygenated ocean conditions correlates temporally with the rise of vascular land plants, and specifically with putative increases in the depth and intensity of rooting in terrestrial ecosystems (e.g., Wallace et al. 2017). In particular, there is a striking coincidence between the emergence of deep rooting systems during the Silurian–Devonian transition (~410–390 Mya) and an increase in the proportion of marine sedimentary rock samples deposited under oxygenated waters (Dahl et al. 2010, Sperling et al. 2015, Stolper & Keller 2018). There also

appear to be changes in samples deposited under anoxic bottom waters, with a shift from samples being dominated by ferruginous conditions to being dominated by euxinic conditions (Sperling et al. 2021). Given this temporal correspondence, it has been hypothesized that vascular plants—by both increasing the mobilization of bioavailable phosphorus from Earth's crust and increasing the globally integrated rate of carbon burial per unit phosphorus—drove a secular increase and long-term stabilization of atmospheric pO_2 at roughly modern values (Kump 1988, Lenton et al. 2016), which would have driven more pervasive oxygenation of the ocean interior. Although the precise mechanistic links among the various stages of terrestrial ecosystem expansion, ocean–atmosphere O_2 and CO_2 levels, and ocean oxygenation remain topics for future work (D'Antonio et al. 2020, Dahl & Arens 2020, Ibarra et al. 2019), it seems increasingly likely that the oceans did not transition into a modern, well-oxygenated ocean until late in Earth's history (<400 Ma), after the initial emergence of land plants.

6. DEOXYGENATION IN OXIC OCEANS: THE MESOZOIC AND CENOZOIC EARTH

It is anticipated that climate warming in the coming centuries will strongly impact a wide range of marine processes, including large-scale circulation, marine biogeochemical cycling, and ecosystem structure (Gruber 2011, Keeling et al. 2010, Levin 2018, Oschlies et al. 2018). These changes have the potential to affect ocean oxygenation in at least three key ways. First, there is a decrease in the solubility of O_2 in marine surface waters as ocean temperatures rise, which will tend to reduce the thermodynamic capacity of the ocean to store dissolved O_2. Second, patterns of ocean circulation are expected to shift considerably in the face of climate warming, leading to the potential for more intense stratification in the shallow ocean and potentially changes in the strength of the large-scale overturning circulation, all of which can both impact the replenishment of dissolved O_2 in the ocean interior and change the supply rates of key nutrients to the surface ocean. Third, changes in the background and seasonal temperatures of marine ecosystems are expected to impact marine biogeochemistry, in particular by modulating rates of photosynthetic O_2 production and the consumption of O_2 during respiration in the ocean interior. However, there remains considerable uncertainty in the overall magnitude and spatial patterns of ocean deoxygenation in the face of future climate warming, with attendant unpredictability in ocean carbon storage, food security, and ecosystem stability (e.g., Bindoff et al. 2019). As a result, there is considerable interest in reconstructing the response of ocean oxygenation to climate shifts in Earth's recent past.

It is useful to distinguish between two different modes of climate shift observed in the Mesozoic (~251–65 Mya) and Cenozoic (~65 Mya to the present) Earth system, which has been characterized by relatively well-oxygenated oceans overall. The first involves long-term secular changes in surface temperature and climate state on timescales greater than $\sim 10^7$ years. For example, over the last ~50 million years, global average surface temperatures have steadily decreased from nearly 30°C during the early Eocene (Burke et al. 2018, Hansen et al. 2013) to less than 10°C during the most recent Pleistocene glacial epoch (e.g., Tierney et al. 2020). The solubility impact of such a large temperature change alone would be anticipated to lead to significant changes in ocean oxygen storage (**Figure 8**), with the prediction of expanded marine anoxia during the warm Eocene. Interestingly, however, there is very little evidence for major changes in ocean oxygenation over the last ~50 million years. For example, metal isotope systematics limit the extent of benthic anoxia to less than ~1% of global seafloor area over the same interval (Wang et al. 2016). This suggests that on long timescales, there are feedbacks within well-oxygenated oceans that

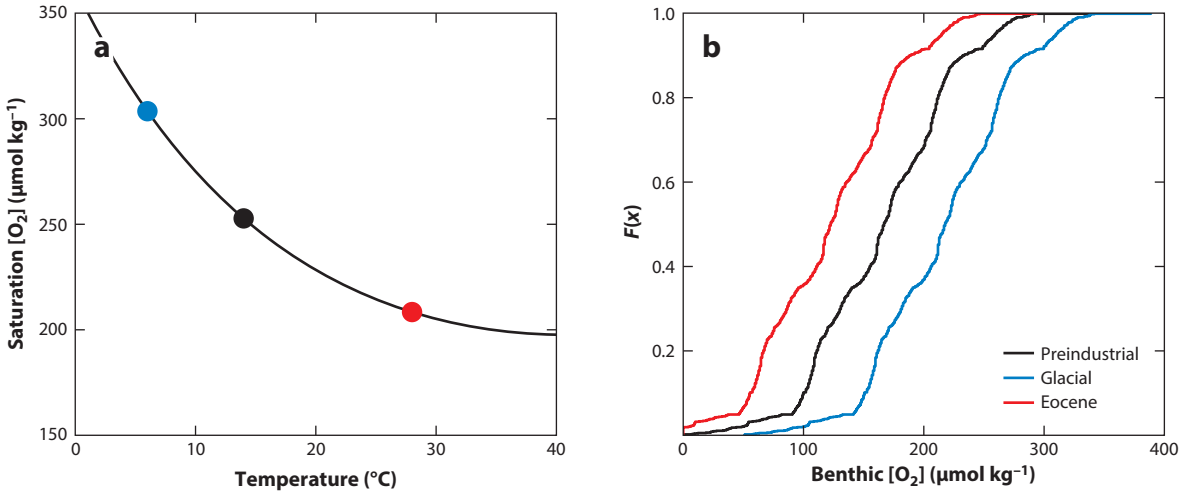

Figure 8

The potential impact of Cenozoic temperature change on ocean oxygenation. (*a*) Dissolved [O_2] at air saturation as a function of temperature and a fixed salinity of 35‰ and pressure of 1 atm using the method of Garcia & Gordon (1992). The circles depict approximate globally averaged surface temperatures for three different Earth system states: the preindustrial modern state (*black*), the Pliocene glacial Earth (*blue*), and the early Eocene Earth (*red*). (*b*) Cumulative frequency distribution of bottom-water dissolved [O_2] in a three-dimensional Earth system model, using a preindustrial modern state (*black*) and scaling [O_2] according to the estimated temperature-dependent changes in solubility shown in panel *a*.

stabilize the carbon, nitrogen, phosphorus, and O_2 cycles and prevent widespread changes to ocean oxygenation despite very large long-term changes to global temperature (e.g., Shackleton 1987).

In marked contrast to protracted secular climate cooling over the last ~50 million years, rapid temperature changes during transient carbon cycle perturbations appear to cause significant increases in the extent of marine anoxia (**Figure 9**). Prominent examples include the Cretaceous and Triassic ocean anoxic events at approximately 92, 120, and 180 Mya and the end-Triassic (~200 Mya) and end-Permian (~250 Ma) mass extinction events, both of which led to staggering losses of marine biodiversity (Dal Corso et al. 2020, Erwin 1990, Fan et al. 2020). Combined estimates of global ocean oxygenation (from uranium isotope records) and carbon release rates (from carbon isotope records and volcanic province eruption rates) indicate a broad scaling between carbon release rate and the intensity of transient ocean deoxygenation (**Figure 9**). The end-Permian is the most extreme of these events, with anoxic conditions estimated to have covered ~30% of global seafloor area, and with anoxic conditions observed even in open-ocean pelagic localities (Isozaki 1997). However, although lower oxygen solubility and intensified ocean stratification can be important drivers of ocean deoxygenation (see above), current state-of-the-art Earth system models forced by temperature changes alone (Penn et al. 2018) do a poor job of predicting the spatial pattern of anoxic conditions (Eltom et al. 2017; Huang et al. 2017, 2019; Isozaki 1997; Lei et al. 2017). This suggests that co-occurring changes to global nutrient cycling, such as increased chemical weathering and phosphorus release to the oceans at elevated temperature and circulation-driven changes to the recycling of nutrients within marine ecosystems, also play key roles in driving ocean deoxygenation during transient climate warming. Further exploration of short- and long-term feedbacks within the coupled carbon, nitrogen, phosphorus, sulfur, and O_2 cycles will be critical for evaluating whether there are suitable past analogs for future ocean deoxygenation.

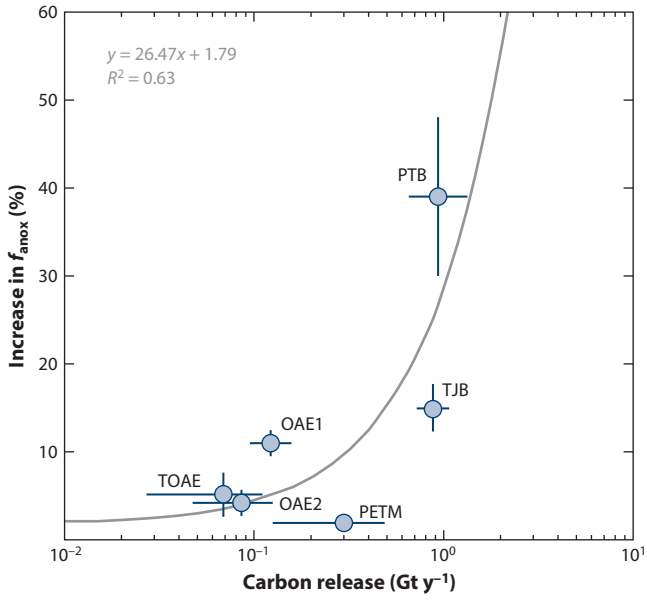

Figure 9

Relationship between the magnitude of carbon cycle perturbation and the transient increase in deep-ocean anoxia for a series of warming events in Earth's Mesozoic/Cenozoic history. Carbon release rates are estimated from carbon isotope data or radiometric constraints on volcanic CO_2 degassing; the relative fraction of seafloor anoxia (f_{anox}) is estimated based on stable uranium isotope records. Abbreviations: OAE, oceanic anoxic event; PETM, Paleocene–Eocene thermal maximum; PTB, Permian–Triassic boundary; TJB, Triassic–Jurassic boundary; TOAE, Toarcian oceanic anoxic event. Data are from C.K. Chen, I.P. Montanez, S. Zhang, T.T. Isson, S.I. Macarewich, et al. (manuscript in review).

SUMMARY POINTS

1. Large-scale patterns of ocean oxygenation are driven fundamentally by the combined effects of the partial pressure of O_2 (pO_2) in the atmosphere and marine nutrient availability. The oxygenation of Earth's oceans has thus followed largely in step with secular increases in atmospheric pO_2 and co-occurring changes to marine nutrient abundance.
2. When atmospheric pO_2 is very low, ocean oxygenation is limited to the surface ocean and is spatially heterogeneous. However, the overall magnitude of disequilibrium between local dissolved [O_2] and the global atmosphere is governed by patterns of ocean circulation and marine nutrient availability.
3. When atmospheric pO_2 surpasses ~10% of the present atmospheric level, surface-ocean oxygenation is poised close to equilibrium with respect to air–sea gas exchange, while strong heterogeneity in oxygenation shifts from the ocean surface to the ocean interior.
4. Atmospheric pO_2 and marine nutrient availability are mechanistically linked, such that low-O_2, high-productivity Earth system states are unlikely to be stable unless geophysical reductant fluxes are large. One result is the possibility that regions of the ocean interior could become weakly oxygenated despite relatively low atmospheric pO_2.

5. Despite evidence for step changes in the background state of the marine redox landscape, there have been significant transient ocean oxygenation and deoxygenation events through the Proterozoic and Phanerozoic.

FUTURE ISSUES

1. The scaling between atmospheric pO_2 and the ocean PO_4^{3-} inventory is a critical feature of the Earth system but is poorly known at present. In particular, although it is conventionally thought that anoxic and sulfidic (euxinic) conditions will lead to more efficient recycling of PO_4^{3-} and the potential for positive feedback during transient ocean deoxygenation, the impact of anoxic and iron-rich (ferruginous) conditions on marine PO_4^{3-} is not well constrained.
2. Similarly, the quantitative scaling between marine SO_4^{2-} abundance and patterns of ocean oxygenation is only broadly constrained. This is important, because some of the most informative proxies for ocean oxygenation in Earth's most distant past come only indirectly from geochemical tracers of ocean SO_4^{2-} abundance.
3. Earth system models that fully encapsulate the coupled oceanic cycles of iron, phosphorus, sulfur, and O_2 across a wide range of redox states will be crucial for better understanding the modalities of ocean oxygenation when atmospheric pO_2 is low and for predicting the dynamics of ocean deoxygenation when atmospheric pO_2 is high.
4. There has been significant focus on the development of new tracer systems and isotopic proxies. Moving forward, an increased focus should be placed on generating robust geochemical records with better context and more directly coupling mechanistic biogeochemical models with observations from Earth's rock record.

DISCLOSURE STATEMENT

The authors are not aware of any affiliations, memberships, funding, or financial holdings that might be perceived as affecting the objectivity of this review.

ACKNOWLEDGMENTS

The authors gratefully acknowledge financial support from the Alfred P. Sloan Foundation, the National Science Foundation, and the National Aeronautics and Space Administration.

LITERATURE CITED

Anbar AD, Duan Y, Lyons TW, Arnold GL, Kendall B, et al. 2007. A whiff of oxygen before the Great Oxidation Event? *Nature* 317:1903–6

Anbar AD, Holland HD. 1992. The photochemistry of manganese and the origin of banded iron formations. *Geochim. Cosmochim. Acta* 56:2595–603

Bar-On YM, Phillips R, Milo R. 2018. The biomass distribution on Earth. *PNAS* 115:6506–11

Bekker A, Kaufman AJ, Karhu JA, Eriksson KA. 2005. Evidence for Paleoproterozoic cap carbonates in North America. *Precambr. Res.* 137:167–206

Bellefroid EJ, Hood AVS, Hoffman PF, Thomas MD, Reinhard CT, Planavsky NJ. 2018. Constraints on Paleoproterozoic atmospheric oxygen levels. *PNAS* 115:8104–9

Bellefroid EJ, Planavsky NJ, Hood AVS, Halverson GP, Spokas K. 2019. Shallow water redox conditions of the mid-Proterozoic Muskwa Assemblage, British Columbia, Canada. *Am. J. Sci.* 319:122–57

Berry WBN, Wilde P. 1978. Progressive ventilation of the oceans—an explanation for the distribution of the lower Paleozoic black shales. *Am. J. Sci.* 278:257–75

Bindoff NL, Cheung WWL, Kairo JG, Arístegui J, Guinder VA, et al. 2019. Changing ocean, marine ecosystems, and dependent communities. In *IPCC Special Report on the Ocean and Cryosphere in a Changing Climate*, ed. HO Pörtner, DC Roberts, V Masson-Delmonte, P Zhai, M Tignor, et al., pp. 447–587. Geneva: Intergov. Panel Clim. Change

Bjerrum CJ, Canfield DE. 2002. Ocean productivity before about 1.9 Ga ago limited by phosphorus adsorption onto iron oxides. *Nature* 417:159–62

Blättler CL, Claire MW, Prave AR, Kirsimäe K, Higgins JA, et al. 2018. Two-billion-year-old evaporites capture Earth's great oxidation. *Science* 360:320–23

Boyer TP, Garcia HE, Locarnini RA, Zweng MM, Mishonov AV, et al. 2018. *World Ocean Atlas 2018*. Data Set, Natl. Cent. Environ. Inf., Natl. Ocean. Atmos. Adm., Silver Spring, MD. **https://www.ncei.noaa.gov/products/world-ocean-atlas**

Burke KD, Williams JW, Chandler MA, Haywood AM, Lunt DJ, Otto-Bliesner BL. 2018. Pliocene and Eocene provide best analogs for near-future climates. *PNAS* 115:13288–93

Busigny V, Lebaeu O, Ader M, Krapez B, Bekker A. 2013. Nitrogen cycle in the late Archean ferruginous ocean. *Chem. Geol.* 362:115–30

Busigny V, Planavsky NJ, Jézéquel D, Crowe S, Louvat P, et al. 2014. Iron isotopes in an Archean ocean analogue. *Geochim. Cosmochim. Acta* 133:443–62

Canfield DE. 2005. The early history of atmospheric oxygen: homage to Robert A. Garrels. *Annu. Rev. Earth Planet. Sci.* 33:1–36

Canfield DE, Ngombi-Pemba L, Hammarlund EU, Bengston S, Chaussidon M, et al. 2015. Oxygen dynamics in the aftermath of the Great Oxidation of Earth's atmosphere. *PNAS* 110:16736–41

Cole DB, Ozaki K, Reinhard CT. 2021. Atmospheric oxygen abundance, marine nutrient availability, and organic carbon fluxes to the seafloor. *Earth and Space Science Open Archive*. **https://www.essoar.org/doi/10.1002/essoar.10506930.1**

Croal LR, Johnson CM, Beard BL, Newman DK. 2004. Iron isotope fractionation by Fe(II)-oxidizing photoautotrophic bacteria. *Geochim. Cosmochim. Acta* 68:1227–42

Crockford PW, Hayles JA, Bao H, Planavsky NJ, Bekker A, et al. 2018. Triple oxygen isotope evidence for limited mid-Proterozoic primary productivity. *Nature* 559:613–16

Czaja AD, Johnson CM, Roden EE, Beard BL, Voegelin AR, et al. 2012. Evidence for free oxygen in the Neoarchean ocean based on coupled iron-molybdenum isotope fractionation. *Geochim. Cosmochim. Acta* 86:118–37

Dahl TW, Arens SKM. 2020. The impacts of land plant evolution on Earth's climate and oxygenation state – an interdisciplinary review. *Chem. Geol.* 547:119665

Dahl TW, Connelly JN, Li D, Kouchinsky A, Gill BC, et al. 2019. Atmosphere-ocean oxygen and productivity dynamics during early animal radiations. *PNAS* 116:19352–61

Dahl TW, Hammarlund EU, Anbar AD, Bond DPG, Gill BC, et al. 2010. Devonian rise in atmospheric oxygen correlated to the radiations of terrestrial planets and large predatory fish. *PNAS* 107:17911–15

Dal Corso J, Bernardi M, Sun Y, Song H, Seyfullah LJ, et al. 2020. Extinction and dawn of the modern world in the Carnian (Late Triassic). *Sci. Adv.* 6:eaba0099

D'Antonio MP, Ibarra DE, Boyce CK. 2020. Land plant evolution decreased, rather than increased, weathering rates. *Geology* 48:29–33

David LA, Alm EJ. 2011. Rapid evolutionary innovation during an Archaean genetic expansion. *Nature* 469:93–96

Daye M, Klepac-Ceraj V, Pajusalu M, Rowland S, Ferrell-Sherman A, et al. 2019. Light-driven anaerobic microbial oxidation of manganese. *Nature* 576:311–14

Derry LA. 2015. Causes and consequences of mid-Proterozoic anoxia. *Geophys. Res. Lett.* 42:8538–46

Dimroth E, Chauvel J-J. 1973. Petrography of the Sokoman Iron Formation in part of the Central Labrador Trough, Quebec, Canada. *Geol. Soc. Am. Bull.* 84:111–34

Doyle KA, Poulton SW, Newton RJ, Podkovyrov VN, Bekker A. 2018. Shallow water anoxia in the Mesoproterozoic ocean: evidence from the Bashkir Meganticlinorium, Southern Urals. *Precambr. Res.* 317:196–210

Eltom H, Abdullatif OM, Babalola LO. 2017. Redox conditions through the Permian-Triassic transition in the upper Khuff formation, Saudi Arabia. *Palaeogeogr. Palaeoclimatol. Palaeoecol.* 472:203–15

Erwin DH. 1990. The end-Permian mass extinction. *Annu. Rev. Ecol. Syst.* 21:69–91

Fakhraee M, Hancisse O, Canfield DE, Crowe SA, Katsev S. 2019. Proterozoic seawater sulfate scarcity and the evolution of ocean-atmosphere chemistry. *Nat. Geosci.* 12:375–80

Falkowski PG, Fenchel T, Delong EF. 2008. The microbial engines that drive Earth's biogeochemical cycles. *Science* 320:1034–39

Fan J, Shen SZ, Erwin DH, Sadler PM, MacLeod N, et al. 2020. A high-resolution summary of Cambrian to Early Triassic marine invertebrate biodiversity. *Science* 367:272–77

Farquhar J, Bao H, Thiemens M. 2000. Atmospheric influence of Earth's earliest sulfur cycle. *Science* 289:756–58

Fralick P, Davis DW, Kissin SA. 2002. The age of the Gunflint Formation, Ontario, Canada: single zircon U-Pb age determinations from reworked volcanic ash. *Can. J. Earth Sci.* 39:1085–91

Garcia HE, Gordon LI. 1992. Oxygen solubility in seawater: better fitting equations. *Limnol. Oceanogr.* 37:1307–12

Garvin J, Buick R, Anbar AD, Arnold GL, Kaufman AJ. 2009. Isotopic evidence for an aerobic nitrogen cycle in the latest Archean. *Science* 323:1045–48

Geyman EC, Maloof AC. 2019. A diurnal carbon engine explains ^{13}C-enriched carbonates without increasing global production of oxygen. *PNAS* 116:24433–39

Gill BC, Lyons TW, Young SA, Kump LR, Knoll AH, Saltzman MR. 2011. Geochemical evidence for widespread euxinia in the Later Cambrian ocean. *Nature* 469:80–83

Godfrey LV, Falkowski PG. 2009. The cycling and redox state of nitrogen in the Archaean ocean. *Nat. Geosci.* 2:725–29

Goldberg T, Archer C, Vance D, Poulton SW. 2009. Mo isotope fractionation during adsorption to Fe (oxyhydr)oxides. *Geochim. Cosmochim. Acta* 73:6502–16

Gregory BS, Claire MW, Rugheimer S. 2021. Photochemical modelling of atmospheric oxygen levels confirms two stable states. *Earth Planet. Sci. Lett.* 561:116818

Grotzinger JP, Kasting JF. 1993. New constraints on Precambrian ocean composition. *J. Geol.* 101:235–43

Gruber N. 2011. Warming up, turning sour, losing breath: ocean biogeochemistry under global change. *Philos. Trans. R. Soc. A* 369:1980–96

Guilbaud R, Poulton SW, Butterfield NJ, Zhu M, Shields-Zhou GA. 2015. A global transition to ferruginous conditions in the early Neoproterozoic oceans. *Nat. Geosci.* 8:466–70

Hansen J, Sato M, Russell G, Kharecha P. 2013. Climate sensitivity, sea level and atmospheric carbon dioxide. *Philos. Trans. R. Soc. A* 371:20120294

Haqq-Misra J, Kasting JF, Lee S. 2011. Availability of O_2 and H_2O_2 on pre-photosynthetic Earth. *Astrobiology* 11:293–302

Hodgskiss MSW, Crockford PW, Peng Y, Wing BA, Horner TJ. 2019. A productivity collapse to end Earth's Great Oxidation. *PNAS* 116:17207–12

Holland HD. 1984. *The Chemical Evolution of the Atmosphere and Ocean*. Princeton, NJ: Princeton Univ. Press

Huang Y, Chen Z, Algeo TJ, Zhao L, Baud A, et al. 2019. Two-stage marine anoxia and biotic response during the Permian-Triassic transition in Kashmire, northern India: pyrite framboid evidence. *Glob. Planet. Change* 172:124–39

Huang Y, Chen Z, Wignall PB, Zhao L. 2017. Latest Permain to Middle Triassic redox condition variations in ramp settings, South China: pyrite framboid evidence. *GSA Bull.* 129:229–43

Ibarra DE, Caves Rugenstein JK, Bachan A, Baresch A, Lau KV, et al. 2019. Modeling the consequences of land plant evolution on silicate weathering. *Am. J. Sci.* 319:1–43

Isozaki Y. 1997. Permo-Triassic boundary superanoxia and stratified superocean: records from lost deep sea. *Science* 276:235–38

Jabłońska J, Tawfik DS. 2021. The evolution of oxygen-utilizing enzymes suggests early biosphere oxygenation. *Nat. Ecol. Evol.* 5:442–48

Johnson JE, Gerpheide A, Lamb MP, Fischer WW. 2014. O_2 constraints from Paleoproterozoic detrital pyrite and uraninite. *GSA Bull.* 126:813–30

Johnson JE, Webb SM, Thomas K, Ono S, Kirschvink JL, Fischer WW. 2013. Manganese-oxidizing photosynthesis before the rise of cyanobacteria. *PNAS* 110:11238–43

Johnston DT. 2011. Multiple sulfur isotopes and the evolution of Earth's surface sulfur cycle. *Earth-Sci. Rev.* 106:161–83

Jones C, Nomosatryo S, Crowe SA, Bjerrum CJ, Canfield DE. 2015. Iron oxides, divalent cations, silica, and the early earth phosphorus crisis. *Geology* 43:135–38

Karhu JA, Holland HD. 1996. Carbon isotopes and the rise of atmospheric oxygen. *Geology* 24:867–70

Karstensen J, Stramma L, Visbeck M. 2008. Oxygen minimum zones in the easter tropical Atlantic and Pacific oceans. *Prog. Oceanogr.* 77:331–50

Kasting JF. 1991. Box models for the evolution of atmospheric oxygen: an update. *Palaeogeogr. Palaeoclimatol. Palaeoecol.* 97:125–31

Kasting JF, Liu SC, Donahue TM. 1979. Oxygen levels in the prebiological atmosphere. *J. Geophys. Res.* 84:3097–107

Kaufman AJ, Johnston DT, Farquhar J, Masterson AL, Lyons TW, et al. 2007. Late Archean biospheric oxygenation and atmospheric evolution. *Science* 317:1900–3

Keeling RF, Körtzinger A, Gruber N. 2010. Ocean deoxygenation in a warming world. *Annu. Rev. Mar. Sci.* 2:199–229

Kendall B, Creaser RA, Reinhard CT, Lyons TW, Anbar AD. 2015a. Transient episodes of mild environmental oxygenation and oxidative continental weathering during the late Archean. *Sci. Adv.* 1:e1500777

Kendall B, Komiya T, Lyons TW, Bates SM, Gordon GW, et al. 2015b. Uranium and molybdenum isotope evidence for an episode of widespread ocean oxygenation during the late Ediacaran Period. *Geochim. Cosmochim. Acta* 156:173–93

Koehler MC, Buick R, Kipp MA, Stüeken EE, Zaloumis J. 2018. Transient surface ocean oxygenation recorded in the ~2.66-Ga Jeerinah Formation, Australia. *PNAS* 115:7711–16

Konhauser KO, Lalonde SV, Amskold L, Holland HD. 2007. Was there really an Archean phosphate crisis? *Science* 315:1234

Kump LR. 1988. Terrestrial feedback in atmospheric oxygen regulation by fire and phosphorus. *Nature* 335:152–54

Kump LR. 2008. The rise of atmospheric oxygen. *Nature* 451:277–78

Kurzweil F, Claire M, Thomazo C, Peters M, Hannington M, Strauss H. 2013. Atmospheric sulfur rearrangement 2.7 billion years ago: evidence for oxygenic photosynthesis. *Earth Planet. Sci. Lett.* 366:17–26

Kurzweil F, Wille M, Gantert N, Beukes NJ, Schoenberg R. 2016. Manganese oxide shuttling in pre-GOE oceans – evidence from molybdenum and iron isotopes. *Earth Planet. Sci. Lett.* 452:69–78

Laakso TA, Schrag DP. 2017. A theory of atmospheric oxygen. *Geobiology* 15:366–84

Lei L, Shen J, Li C, Algeo TJ, Chen Z, et al. 2017. Controls on regional marine redox evolution during Permian-Triassic transition in South China. *Palaeogeogr. Palaeoclimatol. Palaeoecol.* 486:17–32

Lenton TM, Dahl TW, Daines SJ, Mills BJW, Ozaki K, et al. 2016. Earliest land plants created modern levels of atmospheric oxygen. *PNAS* 113:9704–9

Lenton TM, Daines SJ, Mills BJW. 2018. COPSE reloaded: an improved model of biogeochemical cycling over Phanerozoic time. *Earth-Sci. Rev.* 178:1–28

Levin LA. 2018. Manifestation, drivers, and emergence of open ocean deoxygenation. *Annu. Rev. Mar. Sci.* 10:229–60

Little CTS, Johannessen KC, Bengston S, Chan CS, Ivarsson M, et al. 2021. A late Paleoproterozoic (1.74 Ga) deep-sea, low-temperature, iron-oxidizing microbial hydrothermal vent community from Arizona, USA. *Geobiology* 19:228–49

Liu A, Tang D, Shi X, Zhou X, Zhou L, et al. 2020. Mesoproterozoic oxygenated deep seawater recorded by early diagenetic carbonate concretions from the Member IV of the Xiamaling Formation, North China. *Precambr. Res.* 341:105667

Liu X, Kah LC, Knoll AH, Cui H, Wang C, et al. 2021. A persistently low level of atmospheric oxygen in Earth's middle age. *Nat. Commun.* 12:351

Lu W, Ridgwell A, Thomas E, Hardisty DS, Luo G, et al. 2018. Late inception of a resiliently oxygenated upper ocean. *Science* 361:174–77

Luo G, Junium CK, Izon G, Ono S, Beukes NJ, et al. 2018. Nitrogen fixation sustained productivity in the wake of the Palaeoproterozoic Great Oxidation Event. *Nat. Commun.* 9:978

Lyons TW, Reinhard CT, Planavsky NJ. 2014. The rise of oxygen in Earth's early ocean and atmosphere. *Nature* 506:307–15

Mänd K, Lalonde SV, Robbins LJ, Thoby M, Paiste K, et al. 2020. Palaeoproterozoic oxygenated oceans following the Lomagundi-Jatuli Event. *Nat. Geosci.* 13:302–6

Marsh R, Müller SA, Yool A, Edwards NR. 2011. Incorporation of the C-GOLDSTEIN efficient climate model into the GENIE framework: "eb_go_gs" configurations of GENIE. *Geosci. Model Dev.* 4:957–92

Meadows VS, Reinhard CT, Arney GN, Parenteau MN, Schwieterman EW, et al. 2018. Exoplanet biosignatures: understanding oxygen as a biosignature in the context of its environment. *Astrobiology* 18:630–62

Melezhik VA, Fallick AE, Rychanchik DV, Kuznetsov AB. 2005. Paleoproterozoic evaporites in Fennoscandia: implications for seawater sulfate, the rise of atmospheric oxygen and local amplification of the $\delta^{13}C$ excursion. *Terra Nova* 17:141–48

Och LM, Shields-Zhou GA. 2012. The Neoproterozoic oxygenation event: environmental perturbations and biogeochemical cycling. *Earth-Sci. Rev.* 110:26–57

Olson SL, Kump LR, Kasting JF. 2013. Quantifying the areal extent and dissolved oxygen concentrations of Archean oxygen oases. *Chem. Geol.* 362:35–43

Olson SL, Schwieterman EW, Reinhard CT, Lyons TW. 2018. Earth: atmospheric evolution of a habitable planet. In *Handbook of Exoplanets*, ed. H Deeg, J Belmonte, pp. 1–37. Cham, Switz.: Springer

Ono S, Kaufman AJ, Farquhar J, Sumner DY, Beukes NJ. 2009. Lithofacies control on multiple-sulfur isotope records and Neoarchean sulfur cycles. *Precambr. Res.* 169:58–67

Oschlies A, Brandt P, Stramma L, Schmidtko S. 2018. Drivers and mechanisms of ocean oxygenation. *Nat. Geosci.* 11:467–73

Ossa Ossa F, Hofmann A, Vidal O, Kramers JD, Belyanin G, Cavalazzi B. 2016. Unusual manganese enrichment in the Mesoarchean Mozaan Group, Pongola Supergroup, South Africa. *Precambr. Res.* 281:414–33

Ossa Ossa F, Hofmann A, Wille M, Spangenberg JE, Bekker A, et al. 2018. Aerobic iron and manganese cycling in a redox-stratified Mesoarchean epicontinental sea. *Earth Planet. Sci. Lett.* 500:28–50

Ostrander CM, Nielsen SG, Owens JD, Kendall B, Gordon GW, et al. 2019. Fully oxygenated water columns over continental shelves before the Great Oxidation Event. *Nat. Geosci.* 12:186–91

Ozaki K, Reinhard CT, Tajika E. 2019. A sluggish mid-Proterozoic biosphere and its effect on Earth's redox balance. *Geobiology* 17:3–11

Partin CA, Bekker A, Planavsky NJ, Scott CT, Gill BC, et al. 2013. Large-scale fluctuations in Precambrian atmospheric and oceanic oxygen levels from the record of U in shales. *Earth Planet. Sci. Lett.* 369–370:284–93

Pavlov AA, Kasting JF. 2002. Mass-independent fractionation of sulfur isotopes in Archean sediments: strong evidence for an anoxic Archean atmosphere. *Astrobiology* 2:27–41

Penn JL, Deutsch C, Payne JL, Sperling EA. 2018. Temperature-dependent hypoxia explains biogeography and severity of end-Permian marine mass extinction. *Science* 362:eaat1327

Planavsky NJ, Asael D, Hofmann A, Reinhard CT, Lalonde SV, et al. 2014. Evidence for oxygenic photosynthesis half a billion years before the Great Oxidation Event. *Nat. Geosci.* 7:283–86

Planavsky NJ, Cole DB, Isson TT, Reinhard CT, Crockford PW, et al. 2018a. A case for low atmospheric oxygen levels during Earth's middle history. *Emerg. Top. Life Sci.* 2:149–59

Planavsky NJ, McGoldrick P, Scott CT, Li C, Reinhard CT, et al. 2011. Widespread iron-rich conditions in the mid-Proterozoic ocean. *Nature* 477:448–51

Planavsky NJ, Rouxel OJ, Bekker A, Hofmann A, Little CTS, Lyons TW. 2012. Iron isotope composition of some Archean and Proterozoic iron formations. *Geochim. Cosmochim. Acta* 80:158–69

Planavsky NJ, Rouxel OJ, Bekker A, Shapiro R, Fralick P, Knudsen A. 2009. Iron-oxidizing microbial ecosystems thrived in late Paleoproterozoic redox-stratified oceans. *Earth Planet. Sci. Lett.* 286:230–42

Planavsky NJ, Slack JF, Cannon WF, O'Connell B, Isson TT, et al. 2018b. Evidence for episodic oxygenation in a weakly redox-buffered deep mid-Proterozoic ocean. *Chem. Geol.* 483:581–94

Poulton SW, Fralick PW, Canfield DE. 2010. Spatial variability in oceanic redox structure 1.8 billion years ago. *Nat. Geosci.* 3:486–90

Rasmussen B, Buick R. 1999. Redox state of the Archean atmosphere: evidence from detrital heavy minerals in ca. 3250–2750 Ma sandstones from the Pilbara Craton, Australia. *Geology* 27:115–18

Raye U, Pufahl PK, Kyser TK, Ricard E, Hiatt EE. 2015. The role of sedimentology, oceanography, and alteration on the δ^{56}Fe value of the Sokoman Iron Formation, Labrador Trough, Canada. *Geochim. Cosmochim. Acta* 164:205–20

Reinhard CT, Planavsky NJ, Gill BC, Ozaki K, Robbins LJ, et al. 2017. Evolution of the global phosphorus cycle. *Nature* 541:386–89

Reinhard CT, Planavsky NJ, Olson SL, Lyons TW, Erwin DH. 2016. Earth's oxygen cycle and the evolution of animal life. *PNAS* 113:8933–38

Reinhard CT, Planavsky NJ, Robbins LJ, Partin CA, Gill BC, et al. 2013. Proterozoic ocean redox and biogeochemical stasis. *PNAS* 110:5357–62

Roscoe SM, Minter WEL. 1993. Pyritic paleoplacer gold and uranium deposits. In *Mineral Deposit Modeling*, ed. RV Kirkham, WD Sinclair, RI Thorpe, JM Duke, pp. 103–24. St. John's: Geol. Assoc. Can.

Rye R, Holland HD. 1998. Paleosols and the evolution of atmospheric oxygen: a critical review. *Am. J. Sci.* 298:621–72

Sahoo SK, Planavsky NJ, Jiang G, Kendall B, Owens JD, et al. 2016. Oceanic oxygenation events in the anoxic Ediacaran ocean. *Geobiology* 14:457–68

Sahoo SK, Planavsky NJ, Kendall B, Wang X, Shi X, et al. 2012. Ocean oxygenation in the wake of the Marinoan glaciation. *Nature* 489:546–49

Scholz F. 2018. Identifying oxygen minimum zone-type biogeochemical cycling in Earth history using inorganic geochemical proxies. *Earth-Sci. Rev.* 184:29–45

Schröder S, Bekker A, Beukes NJ, Strauss H, van Niekerk HS. 2008. Rise in seawater sulphate concentration associated with the Paleoproterozoic positive carbon isotope excursion: evidence from sulphate evaporites in the ~2.2–2.1 Gyr shallow-marine Lucknow Formation, South Africa. *Terra Nova* 20:108–17

Scott C, Lyons TW, Bekker A, Shen Y, Poulton SW, et al. 2008. Tracing the stepwise oxygenation of the Proterozoic ocean. *Nature* 452:456–59

Shackleton NJ. 1987. The carbon isotope record of the Cenozoic: history of organic carbon burial and of oxygen in the ocean and atmosphere. *Geol. Soc. Lond. Spec. Publ.* 26:423–34

Shang M, Tang D, Shi X, Zhou L, Zhou X, et al. 2019. A pulse of oxygen increase in the early Mesoproterozoic ocean at ca. 1.57–1.56 Ga. *Earth Planet. Sci. Lett.* 527:115797

Sheen AI, Kendall B, Reinhard CT, Creaser RA, Lyons TW, et al. 2018. A model for the oceanic mass balance of rhenium and implications for the extent of Proterozoic ocean anoxia. *Geochim. Cosmochim. Acta* 227:75–95

Slack JF, Grenne T, Bekker A. 2009. Seafloor-hydrothermal Si-Fe-Mn exhalites in the Pecos greenstone belt, New Mexico, and the redox state of ca. 1720 Ma deep seawater. *Geosphere* 5:302–14

Slack JF, Grenne T, Bekker A, Rouxel OJ, Lindberg PA. 2007. Suboxic deep seawater in the late Paleoproterozoic: evidence from hematitic chert and iron formation related to seafloor-hydrothermal sulfide deposits, central Arizona, USA. *Earth Planet. Sci. Lett.* 255:243–56

Sperling EA, Melchin MJ, Fraser T, Stockey RG, Farrell UC, et al. 2021. A long-term record of early to mid-Paleozoic marine redox change. *Sci. Adv.* 7:eabf4382

Sperling EA, Rooney AD, Hays LE, Sergeev VN, Vorob'eva NG, et al. 2014. Redox heterogeneity of subsurface waters in the Mesoproterozoic ocean. *Geobiology* 12:373–86

Sperling EA, Wolock CJ, Morgan AS, Gill BC, Kunzmann M, et al. 2015. Statistical analysis of iron geochemical data suggests limited late Proterozoic oxygenation. *Nature* 523:451–54

Steele JH. 1974. *The Structure of Marine Ecosystems*. Cambridge, MA: Harvard Univ. Press

Stolper DA, Keller CB. 2018. A record of deep-ocean dissolved O_2 from the oxidation state of iron in submarine basalts. *Nature* 553:323–27

Sun D, Ito T, Bracco A. 2017. Oceanic uptake of oxygen during deep convection events through diffusive and bubble-mediated gas exchange. *Glob. Biogeochem. Cycles* 31:1579–91

Tang D, Shi XY, Wang X, Jiang G. 2016. Extremely low oxygen concentration in mid-Proterozoic shallow seawaters. *Precambr. Res.* 276:145–57

Tierney JE, Zhu J, King J, Malevich SB, Hakim GJ, Poulsen CJ. 2020. Glacial cooling and climate sensitivity revisited. *Nature* 584:569–73

Tyrrell T. 1999. The relative influences of nitrogen and phosphorus on oceanic primary production. *Nature* 400:525–31

van de Velde SJ, Hülse D, Reinhard CT, Ridgwell A. 2021. Iron and sulfur cycling in the cGENIE.muffin Earth system model (v0.9.21). *Geosci. Model Dev.* 14:2713–45

Wallace MW, Hood AVS, Shuster A, Greig A, Planavsky NJ, Reed CP. 2017. Oxygenation history of the Neoproterozoic to early Phanerozoic and the rise of land plants. *Earth Planet. Sci. Lett.* 466:12–19

Wang X, Planavsky NJ, Reinhard CT, Hein JR, Johnson TM. 2016. A Cenozoic seawater redox record derived from $^{238}U/^{235}U$ in ferromanganese crusts. *Am. J. Sci.* 316:64–83

Wei G, Planavsky NJ, Tarhan LG, He T, Wang D, et al. 2020. Highly dynamic marine redox state through the Cambrian explosion highlighted by authigenic $\delta^{238}U$ records. *Earth Planet. Sci. Lett.* 544:116361

Wilde P. 1987. Model of progressive ventilation of the late Precambrian-early Paleozoic ocean. *Am. J. Sci.* 287:442–59

Wright JJ, Konwar KM, Hallam SJ. 2012. Microbial ecology of expanding oxygen minimum zones. *Nat. Rev. Microbiol.* 10:381–94

Wyrtki K. 1962. The oxygen minima in relation to ocean circulation. *Deep-Sea Res.* 9:11–23

Yang S, Kendall B, Lu X, Zhang F, Zheng W. 2017. Uranium isotope compositions of mid-Proterozoic black shales: evidence for an episode of increased ocean oxygenation at 1.36 Ga and evaluation of the effect of post-depositional hydrothermal fluid flow. *Precambr. Res.* 298:187–201

Zahnle KJ, Claire M, Catling D. 2006. The loss of mass-independent fractionation in sulfur due to a Paleoproterozoic collapse of atmospheric methane. *Geobiology* 4:271–83

Zerkle AL, Poulton SW, Newton RJ, Mettam C, Claire MW, et al. 2017. Onset of the aerobic nitrogen cycle during the Great Oxidation Event. *Nature* 542:465–67

Annual Review of Marine Science

Volume 14, 2022

Contents

Errata

An online log of corrections to *Annual Review of Marine Science* articles may be found at http://www.annualreviews.org/errata/marine